Dynamic behavior of quantum cellular automata

P. Douglas Tougaw and Craig S. Lent[a)]
Department of Electrical Engineering, University of Notre Dame, Notre Dame, Indiana 46556

(Received 20 November 1995; accepted for publication 9 July 1996)

We examine the dynamic behavior of quantum cellular automata, arrays of artificial quantum-dot cells that can be used to perform useful computations. The dynamics of the array can be solved directly, retaining the full many-electron degrees of freedom only for small array sizes. For larger arrays, we develop several approximate techniques for reducing the size of the basis set required. We examine the effect of intercellular quantum correlations on the switching response. Several important examples of switching behavior are solved using the techniques developed. © *1996 American Institute of Physics.* [S0021-8979(96)04220-X]

I. INTRODUCTION

Devices based on quantum mechanical principles hold the promise of faster speeds and greatly reduced sizes.[1] Most quantum devices that have been proposed essentially try to reproduce the current switching behavior of conventional transistors and insert quantum devices into conventional transistor-based circuit architectures. For example, one major difficulty shared by many quantum devices has been driving one device with the output of similar devices.[2,3] The input of such a device is typically a voltage which must change by several millivolts, while the change in the output current can be measured in nanoamperes. The unique features of quantum devices require the development of new computer architectures matched to their capabilities and limitations.

We have proposed a new type of device combined with an integrated architecture which we have termed quantum cellular automata (QCA). Experiments are underway to try to realize this system in semiconductors. We have explored the theoretical behavior of QCA arrays in the steady-state regime[4–9] and here extend that analysis to include time-dependent response.

Quantum cellular automata are arrays of Coulomb-coupled quantum-dot cells. Electrons within each cell have well-defined states with different associated charge distributions. The state of each cell is determined by its interaction with neighboring cells through the Coulomb interaction. Tunneling between cells is assumed to be completely suppressed by intercellular barriers. The array is then a many-electron system whose overall state is determined by the boundary conditions on edge cells which act as the input channels. The state of the edge cells can be set by electrostatic interaction with control electrodes. Computation is affected because one can design the layout of the cells so that the ground state of the many-electron problem corresponds to the solution state of the computational problem. We have shown that simple design rules allow the layout of cellular arrays which can perform significant and general computational tasks.[8]

The QCA scheme has many appealing features. Local connectivity through the Coulomb interaction solves the well-known interconnection problem which plagues conventional architectures as device size decreases.[10–19] Edge-driven computation means that power is only supplied at the edges of the device, so neither power nor information needs to be supplied to the interior of the QCA array. As device sizes shrink, the relevant energies increase and higher temperature operation becomes possible. In principle, QCA implementations could be shrunk to the size of molecules.

Needless to say, many questions remain to be worked out concerning the behavior of ideal arrays as well as the many barriers to practical implementation. Most of the work to date has been an investigation of the time-independent nature of QCA arrays.[4–9] Due to the basic device paradigm, the desired result depends only on the ground state of the system. For this reason, it has been important to first study the time-independent behavior of these arrays. We now turn to examining time-independent behavior.

As stated above, the QCA approach is fundamentally concerned with the ground state of the multicell array. The physical ground state is mapped to the logical solution of the problem. The details of the dynamic behavior of the system as it is evolving toward its ground state are secondary to the mapping itself. This is one of the strengths of the QCA approach—the details of the evolution of the system, which may be hard to control, are not essential in getting the computation right. The dynamics of the system are *doing* the computing only in the sense that they move the system to its new ground state. The computing is performed by the relationship of the ground state to the solution state.

Why then is an exploration of the dynamics important? The reasons are twofold. First, it is of interest to try to understand the inherent limits on the switching speed of the device or array. Second, the dynamics could become critical if the system cannot actually get to its ground state because it becomes stuck in a metastable state. In that case, the mapping between the ground state and the solution state is irrelevant because the system never arrives at the ground state.

The actual dynamical evolution of the system is complicated enormously by its contact with the rest of the world. That the system is in contact with the environment is, of course, very important because it is by dissipating energy to the environment that the system relaxes to its ground state. On the other hand, describing this relaxation involves modeling the time evolution of a quantum system in contact with a thermal reservoir. This time evolution then depends on the

[a)]Electronic mail: lent@callisto.ee.nd.edu

 0021-8979/96/80(8)/4722/15/$10.00

specific details of the coupling to the reservoir—for example, the precise coupling through specific phonon modes, and the precise occupancy of those modes. We cannot hope to solve this problem in its entirety.

What *can* be done is to describe two limits of the coupling to the environment. One limit is when the elastic (isoenergetic) evolution of the system takes place on a time scale much longer than the inelastic coupling to the environment. If the coupling to the environment is very strong and effective at coupling the system to its ground state, then the system dynamics can be described simply by the golden-rule rate for scattering from its initial state (just after the inputs are switched) to its final ground state. The inelastic time evolution can then be described by rate equations and the switching times are simply related to these rates. Of course, the rates themselves may be quite difficult to calculate. These *extrinsic* switching times, which depend critically on the nature of the coupling to the thermal environment, need to be determined experimentally for specific realizations of QCA's.

The other limit, the one we focus on here, is when the inelastic coupling to the environment is slower than the elastic time evolution of the system. In this case we can study the dynamics of the isolated system which can be described by a Schrödinger equation. The focus here is on how signals propagate and devices switch when they are *not* dissipating energy to the environment. We refer to the switching times in this regime as *intrinsic* switching times because they result from intercellular dynamics only and not from the coupling to the environment. Though the problem we are addressing is now made simpler by assuming the system is isolated, and therefore described by Schrödinger dynamics, it is nevertheless a many-particle system whose behavior is challenging to capture. The main results of this article are the development of successive levels of approximation to model the dynamic switching response of isolated QCA systems.

Since the ground state behavior of QCA devices determines their geometry and the nature of their operation, it is important to understand the time-independent nature of QCA devices before progressing to a study of their dynamic behavior. For this reason, a review of the time-independent behavior of these devices is given in the next section to provide background for the new material.

We will not explicitly include the measurement apparatus in our description of the dynamics. It has been shown experimentally that the charge state of a dot can be probed noninvasively in the classical sense.[20] By this we mean that one can construct a sensitive electrometer, using either a ballistic constriction near pinchoff or a larger quantum dot, such that the charge in the electrometer has a vanishingly small effect on the energy levels in the dot. Of course, if a measurement is made it cannot be noninvasive in the quantum-mechanical sense—a ''wave function collapse'' will occur. Within the QCA paradigm, however, one only measures the edge cells in the ground state. This would be done over a long length of time compared to the time-scale of interdot quantum fluctuations. Thus, as usual, one measures an expectation value. In any case, our concern here is with exploring the intrinsic dynamics of the array, not the interaction with a measurement scheme.

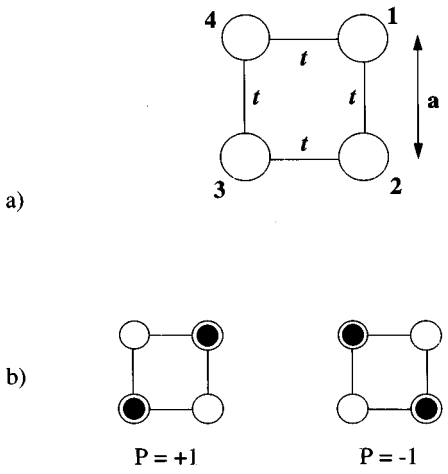

FIG. 1. Schematic of the basic four-site cell. (a) The geometry of the cell. The tunneling energy between two neighboring sites is designated by t, while a is the near-neighbor distance. (b) Coulombic repulsion causes the electrons to occupy antipodal sites within the cell. These two bistable states result in cell polarizations of $P=+1$ and $P=-1$ [see Eq. (2)].

In Sec. III we develop a dynamical description of an array when intercellular correlation effects can be neglected. This is the simplest approach to the dynamics because the dynamics of the array as a whole can then be partitioned cleanly into the dynamics of each cell individually. In fact, correlation effects between cells may be important, so in the next section (Sec. IV) we develop a treatment of array dynamics which treats the entire array as a single quantum system. This involves using the full direct product many-cell basis set. This approach, while ''exact'' in the sense of solving the model we employ, is impractical for all but very small systems. We require some approximations. In Sec. V, the two-state approximation is introduced along with a technique for selecting a reduced basis set. The results of several two-state calculations are shown in Sec. VI. The dynamics of a semi-infinite wire and an energy-absorbing boundary condition are explained in Sec. VII along with the applications of those methods. The scaling of the dynamics with cell size is illustrated in Sec. VIII by considering the switching response of a possible macromolecular QCA implementation. Conclusions and a discussion of the results follow in Sec. IX.

II. CELL BASIS STATES AND STEADY-STATE BEHAVIOR

A schematic diagram of a single QCA cell is shown in Fig. 1(a). This figure shows that a cell consists of four quantum dots arranged in a square pattern. Elsewhere, we have discussed QCA cells with a fifth dot at the center of the square. While such a fifth dot will slightly improve the behavior of the QCA cells, it greatly increases the numerical complexity of the cell model, particularly for calculating dynamic behavior. For this reason, we consider only the four-site cell in this paper. There are two electrons within the cell and tunnel barriers between adjacent sites. Tunneling out of the cell is assumed to be completely suppressed.

QCA cells can be scaled down to atomic dimensions. As cell size is reduced, the energy splitting between stationary states increases and the temporal response becomes faster (as will be seen in Sec. VII). Simple scaling rules can be used to account for these results. To avoid obfuscating actual performance behind dimensionless parameters, we have chosen to focus on a ''standard cell''[7,8] that exhibits robust behavior while remaining within the reach of electron beam nanolithography. We will concentrate largely on such a standard cell here. Undoubtedly, the first experiments will be on larger cells, while final technological promise rests with smaller cells.

The near-neighbor distance between dots within a ''standard cell'' is 20 nm, while the cell centers will be separated by three times this distance. The tunneling energy between dots is 0.3 meV, and the other physical constants of the modeled system correspond to those of GaAs. We have elsewhere examined the full parameter space of tunneling energies and interdot distances.[7]

We use a simple Hamiltonian of the extended-Hubbard type to describe this cell. Each quantum dot is considered only as a site, internal degrees of freedom for the dot being thus ignored. The Hamiltonian employed is given by

$$H^{\text{cell}}=\sum_{i,\sigma}(E_0+V_i)\hat{n}_{i,\sigma}+\sum_{i>j,\sigma}t_{i,j}(\hat{a}^{\dagger}_{i,\sigma}\hat{a}_{j,\sigma}+\hat{a}^{\dagger}_{j,\sigma}\hat{a}_{i,\sigma})+\sum_{i}E_Q\hat{n}_{i,\uparrow}\hat{n}_{i,\downarrow}+\sum_{i>j,\sigma,\sigma'}V_Q\frac{\hat{n}_{i,\sigma}\hat{n}_{j,\sigma'}}{|\mathbf{R}_i-\mathbf{R}_j|}. \tag{1}$$

Here we use the usual second-quantized notation where $\hat{a}_{i,\sigma}(\hat{a}^{\dagger}_{i,\sigma})$ annihilates (creates) an electron on site i with spin σ. The number operator for electrons of spin σ on site i is $\hat{n}_{i,\sigma}=\hat{a}^{\dagger}_{i,\sigma}\hat{a}_{i,\sigma}$. In Eq. (1), the first term represents the on-site energy of each dot. The potential energy of an electron at dot i due to charges outside the cell, including effects of charges in other cells, is V_i. The second term accounts for electron tunneling between sites, with $t_{i,j}=0.3$ meV for neighboring sites and $t_{i,j}=0$ for antipodal sites. The third term is the on-site charging cost to put two electrons of opposite spin on the same dot,[21] and the last term corresponds to the Coulombic interaction between the electrons on different sites within a cell.

For the steady-state problem this Hamiltonian is used in the solution of the time-independent Schrödinger equation,

$$\hat{H}^{\text{cell}}|\psi_i\rangle=E_i|\psi_i\rangle, \tag{2}$$

where $|\psi_i\rangle$ is the i^{th} eigenstate of the Hamiltonian, and E_i is the corresponding eigenvalue. These eigenstates are found using the many-particle site-ket basis for four sites and two electrons of opposite spins

$$|\phi_1\rangle=\left|\begin{matrix}0&0&0&1\\0&0&0&1\end{matrix}\right\rangle,\quad |\phi_2\rangle=\left|\begin{matrix}0&0&0&1\\0&0&1&0\end{matrix}\right\rangle,\ldots,\quad |\phi_{16}\rangle=\left|\begin{matrix}1&0&0&0\\1&0&0&0\end{matrix}\right\rangle. \tag{3}$$

The notation for these basis vectors indicates spin-up electrons in the top row, spin-down electrons in the bottom row, and columns are numbered in the same order as sites within the cell as in Fig. 1(a). Using this notation, a basis vector with a spin-up electron on the first site and a spin-down electron on the third site would be represented by the basis vector

$$|\phi\rangle=\left|\begin{matrix}1&0&0&0\\0&0&1&0\end{matrix}\right\rangle. \tag{4}$$

These basis states, which are the eigenstates of the number operator on a particular site within the cell, will be referred to as the *underlying basis set*. We calculate the Hamiltonian matrix in this underlying basis set by numerically evaluating each matrix element:

$$H_{ij}=\langle\phi_i|\hat{H}|\phi_j\rangle \tag{5}$$

and finding the eigenvectors of the resulting 16×16 matrix.

The ground state of the cell, $|\psi_0\rangle$, is represented in this basis as:

$$|\psi_0\rangle=\sum_j\psi^0_j|\phi_j\rangle. \tag{6}$$

Here, $|\phi_j\rangle$ is the jth underlying basis vector and ψ^0_j is the coefficient of that basis vector, which is found by direct diagonalization of the Hamiltonian.

If the tunneling between cells is relatively small, the electron number is approximately quantized on each of the sites.[22] Qualitatively, it is clear that the ground state of the cell will correspond to the two electrons occupying antipodal sites resulting in a ''polarized'' cell as shown schematically in Fig. 1(b). If the tunneling energies become comparable to the Coulomb energies in the problem, the two-electron wave function becomes delocalized and the cell polarization vanishes.[23] As long as the tunneling matrix elements of the Hamiltonian are small compared to the Coulombic terms, all cells in the array will be very close to one of these two polarized states. In order to make quantitative this notion of cell polarization we define the cell polarization, which is a property of the ground state eigenfunction $|\psi_0\rangle$, as follows:

$$P\equiv\frac{(\rho_1+\rho_3)-(\rho_2+\rho_4)}{\rho_1+\rho_2+\rho_3+\rho_4}. \tag{7}$$

Here, ρ_i is the expectation value of the number operator on site i for the ground state eigenfunction:

$$\rho_i=\langle\psi_0|\hat{n}_i|\psi_0\rangle. \tag{8}$$

As shown schematically in Fig. 1(b), this function yields $P=+1$ for one of the fully polarized states and $P=-1$ for the other. Cells in a combination of these two states will have an intermediate polarization between -1 and $+1$. Due to the bistability of the cell response, it is possible to store a single binary bit in the quantum state of each cell. We will refer to a cell with $P=+1$ as being in the logical ''1'' state, and a cell with $P=-1$ will be in the logical ''0'' state.

It is illuminating to quantify the effect that the state of one cell has on that of its neighbors. We consider two neighboring cells separated by 60 nm and investigate how the polarization of one of the cells affects the polarization of the

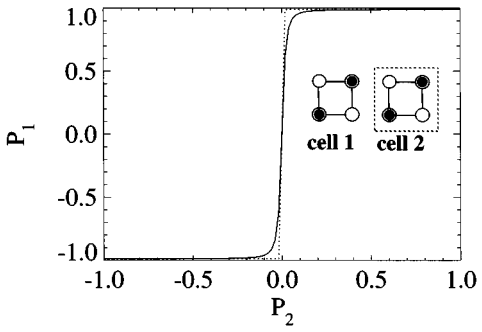

FIG. 2. The cell–cell response. The polarization of cell 2 is fixed and its Coulombic effect on the polarization of cell 1 is measured. The nonlinearity and bistable saturation of this response serves the same role as gain in a conventional digital circuit.

other. In particular, the polarization of cell 2 is fixed at a series of values ranging from -1 to $+1$ and its Coulombic effect on the polarization of cell 1 is computed for each of these values. For each value of the cell 2, the driver cell, the ground state of cell 1 is computed by direct diagonalization of Eq. (1), and the induced polarization calculated from the ground state. The results are shown in Fig. 2, which we refer to as a cell–cell response function. In this figure, the effect of one cell on its neighbors is shown to be very nonlinear and exhibits bistable saturation. Since a very slight polarization of cell 2 induces a much larger polarization in cell 1, cell–cell interaction provides the analogue to gain in a conventional digital circuit, restoring the signal levels at each stage.

The simulation of a device or array containing many cells requires an extension of the single-cell approach. The simplest of these extensions is the intercellular Hartree approximation (ICHA), which has been discussed at length in Ref. 7 and 8. A brief description of this technique will be presented here, but a more thorough presentation can be found in those references.

In this approximation, exchange and correlation effects are included exactly within each cell, but are neglected between cells. Cells within the array interact with each other by affecting the on-site energy term of the Hamiltonian, changing V_i in Eq. (1). The ground state of a particular cell in the array (the ''target'' cell) is calculated under the influence of the polarizations of all other cells in the array which are momentarily fixed. In turn, each of the other cells is also chosen as the target cell, so their polarizations change. This procedure is carried out iteratively and the array relaxes until no further change in any of the cells is observed. In this way, the ground state polarization of every cell in the array can be calculated using only a local Hamiltonian for each cell.

It is important to note that, although the intercellular Hartree approximation can be used to accurately calculate the ground state of an array of QCA cells, it is not capable of determining the dynamic behavior of the array. By its nature, the ICHA is appropriate for ground state calculations, but dynamic response requires the inclusion of many-cell excited states, which are beyond the scope of the approximation. For this reason, it is necessary to develop other techniques to model the time-dependent behavior of many-cell devices.

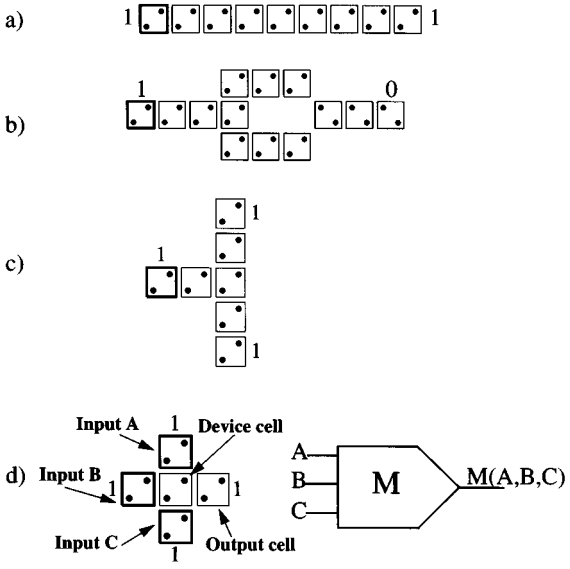

FIG. 3. Fundamental QCA devices. (a) The binary wire allows transmission of information from one point to another within the array. (b) The inverter uses diagonal antivoting behavior to invert the signal. (c) Fanout allows the result of a calculation to be propagated to two or more other points within the array. (d) The majority logic gate is the fundamental logical element of a QCA array.

Figure 3(a) shows the result of such an ICHA calculation performed on a linear array of QCA cells. The cell on the left (with the darker border) is held at a polarization of $P=+1$, and all the other cells in the array are free to react to this polarization. As shown by this figure, the ground state of such a configuration has the polarization of the other cells aligned with the direction of the driver cell. Therefore, such a ''binary wire'' can be used to propagate inputs and intermediate results within the array. As previously mentioned, local fluctuations in polarization due to fabrication irregularities can be overcome by the bistable saturation of cell response.

It is important to note that, unless stated otherwise, the figures shown here are not schematic. Figure 3 shows the actual results of solutions of the ground state using the time-independent Schrödinger equation. Cells with darker borders have fixed polarizations, while cells with lighter borders are free to react to that polarization. The radius of the dot at each site is proportional to the expectation value of the number operator on that site.

Figure 3(b) shows an inverter for a QCA signal. Such inversion is made possible because, while cells in a horizontal or vertical arrangement tend to align with each other, cells in a diagonal arrangement tend to anti-align. Thus, the incoming signal is split into two parts using vertical alignments, then the two parts are rejoined diagonally. The splitting ensures symmetry between inversion of a 1 and inversion of a 0.

As shown in Fig. 3(c), the splitting of a QCA binary wire into two such wires maintains the same signal in each of the two new wires. Such fanout behavior is important, since the result of one intermediate calculation may need to serve as an input for two or more subsequent calculations.

Figure 3(d) presents the most fundamental of QCA logical devices: the majority logic gate. Three inputs, here coming from the top, left, and bottom, are positioned as neighbors of a device cell. The output leaves the device through a binary wire connected to the fourth neighbor of the device cell. The state of the device cell and the output cell (shown here on the right) matches that of a majority of the three inputs. That a single QCA cell serves as a three input majority gate illustrates the potential for revolutionary increases in functional density within the QCA paradigm. Notice, also, that by fixing one of the three inputs, the majority gate can be ''reduced'' to a two-input AND or OR gate. When combined with the inverter, logical completeness is thereby assured.

III. INCOHERENT CELL-CELL DYNAMICS

The simplest approach to the time dependence of an array of cells is to ignore correlations and coherence between cells and solve separate Schrödinger equations for each cell. In this Hartree-type treatment, one treats each cell as responding to the charge on every other cell. Within the cell, the time dependence is determined by the full two-body Hamiltonian. For cell k, we can write the Hamiltonian as

$$H_k^{\text{cell}} = \sum_{i,\sigma} (E_0 + V_i)\hat{n}_{i,\sigma} + \sum_{i>j,\sigma} t_{i,j}(\hat{a}_{i,\sigma}^{\dagger}\hat{a}_{j,\sigma} + \hat{a}_{j,\sigma}^{\dagger}\hat{a}_{i,\sigma}) + \sum_i E_Q \hat{n}_{i,\uparrow}\hat{n}_{i,\downarrow} + \sum_{i>j,\sigma,\sigma'} V_Q \frac{\hat{n}_{i,\sigma}\hat{n}_{j,\sigma'}}{|\mathbf{R}_i - \mathbf{R}_j|} + \sum_{i,j,\sigma,\sigma',m\neq k} V_Q \frac{\hat{n}_{i,\sigma}\rho_{j,\sigma'}(m)}{|\mathbf{R}_i - \mathbf{R}_j(m)|}, \tag{9}$$

where each operator acts only on the electrons within the cell. The electron density due to electrons of spin σ in dot j of cell m is given by the expectation of the number operator for that site:

$$\rho_{j,\sigma}(m) = \langle \psi_m(t)|\hat{n}_{j,\sigma}(m)|\psi_m(t)\rangle. \tag{10}$$

For each cell we can then solve the time-dependent Schrödinger equation

$$H_k^{\text{cell}}|\Psi_k(t)\rangle = i\hbar \frac{\partial}{\partial t}|\Psi_k(t)\rangle. \tag{11}$$

The set of Schrödinger equations given by Eq. (11) are coupled only through the intercell potential terms [the last term in Eq. (9)]. Results of a calculation based on Eqs. (9)–(11) for the switching of an isolated line of cells are shown in Fig. 4. The first cell is switching abruptly from a polarization of -1 (logical 0) to a polarization of $+1$ (logical 1) and the resulting ''kink'' propagates down the line switching subsequent cells.[24] If the line is finite, the kink will reflect at the end of the line and bounce back and forth until inelastic processes which are not included in our treatment relax the system to its new switched ground state.

Limitations of this approach are clear. This treatment ignores correlations between electron states in different cells. Further, Eq. (10) uses an expectation value as an instantaneous charge, when it is in fact an average quantity over the quantum ensemble. Still, this approach could prove useful for a quasistatic regime in which each cell responds to changes in local potential which occur much more slowly than quantum fluctuations (tunneling) within the cells. As we shall see in the following section, the uncorrelated approach yields dynamics which are qualitatively correct but underestimate the intrinsic switching speed of an array. The velocity of the kink is increased by correlation effects between cells.

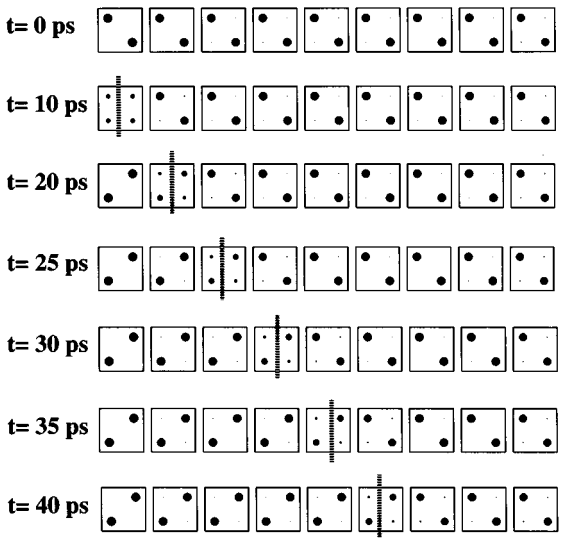

FIG. 4. The time-dependent behavior of a QCA binary wire with no quantum correlations between cells. The polarization kink propagates down the wire at a rate of approximately 5 ps per cell, which is slower than in the fully coherent system.

IV. COHERENT FULL-BASIS CELL DYNAMICS

To treat correlation effects between cells we must model the entire cellular array as a single quantum system. Since there are many particles in the array, this approach has serious practical limitations. In this section we examine the approach that would be used if we were unconstrained by the limits of computational power and could solve the system exactly. Key to the ''correct'' approach is using, as a basis set, the states formed from direct products of individual cell states.

A. The direct-product basis

To construct the basis set for an array of cells, one must take the direct product of all combinations of the single-cell basis vectors. In a single cell with four sites and two electrons of opposite spin, there are a total of sixteen underlying basis vectors. All possible direct product combinations of these sixteen vectors for two cells would yield $16^2 = 256$ basis vectors. In general, an array with N_C number of cells and $N_{\mathbf{V}}$ number of basis vectors within each cell will have a total number of direct-product basis vectors equal to

$$N_{\text{BASIS}} = N_V^{N_C}. \tag{12}$$

An enumeration of these direct product basis vectors for a system with three cells and sixteen underlying vectors is

$$|\Phi_1\rangle = |\phi_1(1)\phi_1(2)\phi_1(3)\rangle,$$
$$|\Phi_2\rangle = |\phi_1(1)\phi_1(2)\phi_2(3)\rangle,$$
$$\vdots$$
$$|\Phi_{17}\rangle = |\phi_1(1)\phi_2(2)\phi_1(3)\rangle,$$
$$\vdots$$
$$|\Phi_{4096}\rangle = |\phi_{16}(1)\phi_{16}(2)\phi_{16}(3)\rangle. \tag{13}$$

Here, the subscript number on each direct-product element refers to the underlying basis ket index and the number in parentheses indicates the cell number. Because operators can now refer to different cells, it is necessary to add an additional parameter to the creation and annihilation operators to specify which cell is being operated upon. The Hamiltonian is also augmented to include intercellular Coulombic interaction:

$$H = \sum_{i,\sigma,m} E_0 \hat{n}_{i,\sigma}(m) + \sum_{i>j,\sigma,m} t_{i,j}(\hat{a}^{\dagger}_{i,\sigma}(m)\hat{a}_{j,\sigma}(m) + \hat{a}^{\dagger}_{j,\sigma}(m)\hat{a}_{i,\sigma}(m)) + \sum_{i,m} E_Q \hat{n}_{i,\uparrow}(m)\hat{n}_{i,\downarrow}(m) + \sum_{i>j,\sigma,\sigma',m} V_Q \frac{\hat{n}_{i,\sigma}(m)\hat{n}_{j,\sigma'}(m)}{|\mathbf{R}_i(m) - \mathbf{R}_j(m)|} + \sum_{i,j,\sigma,\sigma',k>m} V_Q \frac{\hat{n}_{i,\sigma}(m)\hat{n}_{j,\sigma'}(k)}{|\mathbf{R}_i(m) - \mathbf{R}_j(k)|}. \tag{14}$$

When the full direct-product Hamiltonian matrix is calculated in this basis, it is possible to determine the eigenstates of an entire array of cells including all exchange and correlation effects both within each cell and between cells. The elements of the Hamiltonian have the form

$$H_{ij} = \langle \Phi_i | \hat{H} | \Phi_j \rangle \tag{15}$$

and the eigenstates of this many-cell Hamiltonian can be found by solving the equation

$$\sum_j H_{ij} \Psi^k_j = E^k \Psi^k_i. \tag{16}$$

When this matrix equation is solved, the many-cell ground state $|\Psi_0\rangle$ can be written in the direct product basis set

$$|\Psi_0\rangle = \sum_j \Psi^0_j |\Phi_j\rangle. \tag{17}$$

This is the most fundamental and accurate model of the behavior of QCA devices, but Eq. (12) indicates that the size of the basis set will rapidly increase to exceed available computing memory and speed.

B. Full dynamic behavior of a short line

By using Eq. (14) to find the full many-cell Hamiltonian in the direct-product basis set, we can model the dynamic response of a small array of cells without the need for further approximations. To this end, we solve the time-dependent Schrödinger equation,

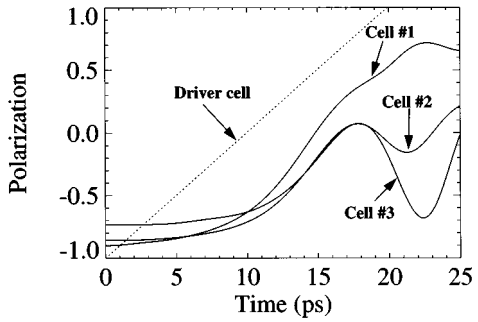

FIG. 5. The dynamic response of a three-cell line using the full direct-product basis set. The dotted line represents the polarization of the driver cell, and the other three cells in the line are indicated. The polarization ''kink'' reflects off the end of the wire because energy dissipation is not included in this model.

$$i\hbar \frac{\partial \Psi}{\partial t} = \hat{H}\Psi \tag{18}$$

in the many-cell direct product basis, $|\Phi_j\rangle$.

Time marching is achieved by finding the projection of the current state on each of the eigenstates of the many-cell Hamiltonian. Each of these projections then propagates forward in time according to the time-dependent Schrödinger equation. Formally,

$$\Psi_j(t+\Delta t) = \langle \Phi_j | \Psi(t+\Delta t)\rangle = \sum_{k,m} \langle \Phi_j | u_k\rangle e^{-i/\hbar (E_k \Delta t)} \langle u_k | \Phi_m\rangle \Psi_m(t), \tag{19}$$

where the $|u_k\rangle$ are the instantaneous eigenstates of the Hamiltonian

$$H(t)|u_k\rangle = E_k |u_k\rangle. \tag{20}$$

When time marching is performed in this way, the wave function remains strictly normalized.

With the available computing power, we are able to model a binary wire with three cells and a driver in this way. Figure 5 shows the result of such a simulation. The polarization of the driver cell (shown as a dotted line) switches continuously from -1 to $+1$ over a period of 20 ps. As that switching occurs, the remaining cells in the line begin to react. The first cell is almost completely switched by the time the polarization kink reaches the end of the short wire. When this happens, the kink reflects because energy dissipation is not included in this model. If it were possible to model a longer line in this way, one would see each cell in the line switching to match the new state of the driver cell.

V. THE TWO-STATE APPROXIMATION

Although the full direct-product basis is the most complete way of modeling QCA devices, it is only possible to model small systems using this scheme. The combinatorial explosion due to Eq. (12) severely limits the size of devices that can be modeled using the full direct-product basis set in this way. For this reason, it is necessary to make reductions in the number of basis vectors used to model larger systems.

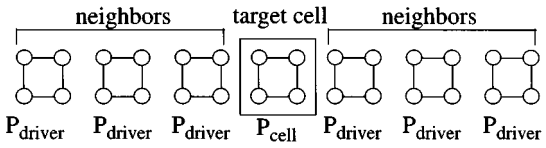

FIG. 6. A schematic representation of the technique used to determine the two self-consistent basis vectors. During each iteration, the polarization of the neighbors is set to match that of the target cell. At convergence, the state of the target cell is that of a cell in the center of a long line of identical cells.

The bistable nature of QCA cells suggests that it is possible to model each cell using only two basis vectors. In this section, we present a technique for selecting two optimal basis vectors and using them to model larger QCA devices.

A. Selection of the two-state basis

When the time-independent behavior of large QCA arrays is modeled as described in Sec. II, it is found that each cell in a line of cells tends to polarize to a particular value of P with a magnitude that may be slightly less than 1. This ''saturation polarization'', P_{sat}, is determined by the size of the cells and the tunneling barriers between dots within the cell. The line will polarize to a state with all cells (except near the end) having polarization $+P_{\mathrm{sat}}$ or $-P_{\mathrm{sat}}$ depending on the sign of the driver polarization at the input. Since each cell naturally tends to a state with these polarizations it is natural to use them as a basis state for describing the system. In order to determine the state vector of a cell exhibiting this saturation polarization, we model a cell in the middle of a long line of similar cells of identical polarization using an iterative technique. Since the cells in an array tend to exhibit this polarization, we will use the state thus calculated as the building block of our two-state basis.

Figure 6 shows a schematic of the system used to determine the saturation polarization state vectors in this way. A target cell is placed in the middle of a linear array of cells with three neighbors on each side. Since the quadrupole interaction of cells decays very rapidly with distance, cells more than three intercellular distances away will have very little effect on each other. For this reason, it is not necessary to include more than three neighbors on each side of the target cell. An iterative process is then carried out to determine the state of the cell in the middle of the wire. At each step of the iterative process, the neighboring cells are held at a polarization equal to that of the target cell. The ground state of the target cell is then calculated by solving the two-electron Schrödinger equation. The driver polarizations are updated to the match the new value of the target cell and the process is repeated until convergence is obtained.

More explicitly, the system starts with the target cell and the neighbors completely polarized in one of the two directions:

$$P_{\mathrm{driver}} = P_{\mathrm{cell}} = \pm 1. \tag{21}$$

The Hamiltonian of the target cell is then calculated as a function of the driver polarizations by adding the effect of the six driver cells to the Hamiltonian of an isolated cell

$$\hat{H}^{\mathrm{cell}}(P_{\mathrm{driver}}) = \hat{H}^{\mathrm{cell}}(0) + V(P_{\mathrm{driver}}). \tag{22}$$

The eigenstates of this Hamiltonian are then calculated:

$$\hat{H}^{\mathrm{cell}}(P_{\mathrm{driver}})|\psi_{\mathrm{cell}}\rangle = E^{\mathrm{cell}}|\psi_{\mathrm{cell}}\rangle. \tag{23}$$

The polarization of the ground state of the target cell can then be found, as in Eqs. (8) and (9), and the polarization of the driver cells is set equal to that calculated for the target cell:

$$P_{\mathrm{driver}} = P_{\mathrm{cell}}. \tag{24}$$

The next iteration begins again at Eq. (22). Once P_{cell} stops changing, we have calculated the state vector of a saturated cell in that polarization direction.

Since each cell can be in either of two polarization directions, we perform this iterative calculation for initial states of both $P=+1$ and $P=-1$. The magnitude of the two saturation polarizations will be the same, but their sign will be different. It is necessary to carry out the calculation twice since the two state vectors thus found will be eigenstates of different Hamiltonians. The polarization at convergence will depend on the initial value given to the polarization of the target and driver cells:

$$\text{initial} \quad P_{\mathrm{driver}} = 1 \Rightarrow P_{\mathrm{sat}}, |\chi_+\rangle \tag{25}$$

and

$$\text{initial} \quad P_{\mathrm{driver}} = -1 \Rightarrow -P_{\mathrm{sat}}, |\chi_-\rangle. \tag{26}$$

The result of this iterative process is the value of P_{sat} and the two vectors $|\chi_+\rangle$ and $|\chi_-\rangle$, which we will use to form the two-dimensional basis for each cell. Each of these is expressed as a superposition of the sixteen underlying basis vectors:

$$|\chi_+\rangle = \sum_j \chi_j^+ |\phi_j\rangle \tag{27}$$

and

$$|\chi_-\rangle = \sum_j \chi_j^- |\phi_j\rangle. \tag{28}$$

Although the two converged states have the same polarization magnitudes and the same eigenenergy, the state vectors $|\chi_+\rangle$ and $|\chi_-\rangle$ are eigenvectors of different Hamiltonians and for this reason they are not orthogonal

$$\hat{H}_{\mathrm{cell}}(P_{\mathrm{sat}})|\chi_+\rangle = E_+^0 |\chi_+\rangle \tag{29}$$

and

$$\hat{H}_{\mathrm{cell}}(-P_{\mathrm{sat}})|\chi_-\rangle = E_-^0 |\chi_-\rangle. \tag{30}$$

We must still explicitly orthogonalize them in order to use them as a convenient basis set. It is also important to maintain symmetry between the two vectors in order to treat the two polarization states on the same footing. If $|\chi_+\rangle$ and $|\chi_-\rangle$ are the two vectors found by the iterative method described above, symmetric orthogonalization requires that $|\chi'_+\rangle$ and $|\chi'_-\rangle$, the corrected vectors, satisfy the following conditions:

$$\langle \chi'_+ | \chi'_- \rangle = 0 \tag{31}$$

and

$$\langle \chi'_+ | \chi_+ \rangle = \langle \chi'_- | \chi_- \rangle. \tag{32}$$

These two criteria are satisfied by the following equations:

$$|\chi'_+\rangle = |\chi_+\rangle - \alpha\beta|\chi_-\rangle \tag{33}$$

and

$$|\chi'_-\rangle = |\chi_-\rangle - \alpha\beta^*|\chi_+\rangle, \tag{34}$$

where

$$\beta = \langle \chi_- | \chi_+ \rangle \tag{35}$$

and

$$\alpha = \frac{1+(1-\beta^2)^{1/2}}{\beta^2}. \tag{36}$$

Once these two symmetric orthogonal basis vectors have been determined for a single cell, we can use their direct-product combinations to model arrays with many cells. Since there are only two basis vectors per cell in this new basis, the total number of basis cells is now

$$N_{\mathrm{BASIS}} = 2^{N_c}. \tag{37}$$

An enumeration of this basis set for a system of three cells is

$$|\Theta_1\rangle = |\chi'_+(1)\chi'_+(2)\chi'_+(3)\rangle,$$

$$|\Theta_2\rangle = |\chi'_+(1)\chi'_+(2)\chi'_-(3)\rangle,$$

$$|\Theta_3\rangle = |\chi'_+(1)\chi'_-(2)\chi'_+(3)\rangle,$$

$$\vdots$$

$$|\Theta_8\rangle = |\chi'_-(1)\chi'_-(2)\chi'_-(3)\rangle. \tag{38}$$

This direct product of the self-consistent symmetric orthogonal basis vectors will simply be referred to as the two-state basis set. It is a direct product of two basis vectors per cell, each of which is a superposition of the sixteen underlying basis vectors.

With this smaller required basis set, it is now possible to perform simulations on arrays with eight to ten cells, which is sufficient to model significant dynamic behavior of QCA's.

B. Validity of reduced basis

The state vector of a single cell exists in a sixteen-dimensional Hilbert space spanned by the underlying basis set [Eq. (3)], but we have now selected a two-dimensional basis set within that space to which the state vector should be largely confined. If the approximation were exact, the state vector would be completely confined to the two-dimensional plane thus defined, so a measurement of that confinement will provide an indication of the accuracy of our approximation.

In order to determine the confinement of the state vector of a cell to the two-dimensional space we have defined, we consider a test case consisting of a single cell with a driver on each side. The polarization of the two drivers is equal, and the value of this polarization is varied between -1 and $+1$. For each value of the driver polarization, the sixteen-dimensional ground state of the cell is calculated. The projection of this ground state onto each of the two basis vectors calculated above is then determined

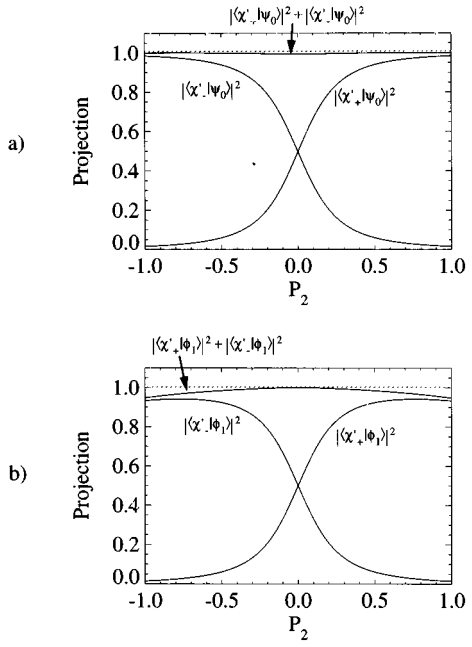

FIG. 7. Projections of the ground state and first excited state onto the chosen two-state basis vectors for varying degrees of cell polarization. (a) Projection of the ground state on each of the two basis vectors and total projection on the two-dimensional space. (b) A similar calculation for the first excited state. The dotted line is plotted at projection=1.

$$\lambda_0^+ = |\langle \chi'_+ | \psi_0 \rangle|^2 \tag{39}$$

and

$$\lambda_0^- = |\langle \chi'_- | \psi_0 \rangle|^2. \tag{40}$$

A similar calculation of the projection is performed for the first excited state of the cell for each value of the driver polarization:

$$\lambda_1^+ = |\langle \chi'_+ | \psi_1 \rangle|^2 \tag{41}$$

and

$$\lambda_1^- = |\langle \chi'_- | \psi_1 \rangle|^2. \tag{42}$$

The results of these calculation are shown in Fig. 7. Figure 7(a) shows the projection of the ground state onto each of the two basis vectors and the total projection into the two-dimensional subspace spanned by $|\chi'_+\rangle$ and $|\chi'_-\rangle$. The minimum value of the total projection into the two-dimensional space is 0.993, which implies that the a typical cell remains almost completely contained within the two-dimensional subspace of the new basis vectors.

Figure 7(b) shows the projection of the first excited state onto each of the basis vectors and the two-dimensional subspace. While the excited states are not important for the time-independent results shown in Sec. II, they are relevant for time-dependent behavior. It is therefore desirable that the first excited state remains mostly in the two-dimensional subspace we have defined, and the minimum projection of 0.947 shows that it does so.

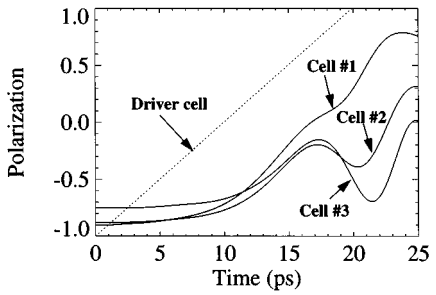

FIG. 8. Dynamic response of a three-cell line using the two-state approximation. The conditions of this simulation are identical to those of Fig. 5, and give very similar results. This agreement highlights the validity of the two-state approximation.

A perhaps more direct measurement of the accuracy of the two-state approximation in reproducing time-dependent results is performed by repeating the calculation of Fig. 5 using the two-state basis set. The result of such a two-state calculation is shown in Fig. 8. All cell parameters and driver conditions are identical to those of Fig. 5, so a comparison of the switching behaviors of the two systems gives a good measure of the accuracy of our approximation.

One can see that the dynamic response of the three-cell wire using the two-state basis is very similar to the same calculation using the full basis set. The polarization of the first cell seems to rise slightly more slowly in the two-state approximation, and the details of the kink reflection are slightly different, but the agreement between the two calculations is very good. This result, combined with that of Fig. 7, gives us some measure of confidence in using the two-state approximation.

C. Mapping to the Ising model

Since only two basis vectors are being used to represent the state of each cell in an array, it is natural, and in fact useful, to consider the relationship of this problem to the Ising spin problem. We begin by rewriting the two-state many-cell basis vectors as

$$|\Theta_j\rangle = |S_1 S_2 S_3 \cdots S_N\rangle, \tag{43}$$

where the pseudo-spin $S_i = +1$ or -1 ($\uparrow$ or $\downarrow$) depending on the presence of χ'_+ or χ'_- in the corresponding position of the original two-state basis vector. One can then evaluate the elements of the Hamiltonian matrix using this new notation

$$H_{ij} = \langle \Theta_i | \hat{H} | \Theta_j \rangle, \tag{44}$$

where $\hat{H}$ is the full many-cell Hamiltonian of Eq. (14). When this Hamiltonian matrix is calculated, one finds that it is of the form:

$$\hat{H} = \frac{E_{\text{kink}}}{2}\left(N - \sum_i S_i S_{i+1}\right) + \sum_i t\hat{\sigma}_x(i), \tag{45}$$

where E_{kink} and t are evaluated numerically using the microscopic Hamiltonian, Eq. (14). The kink energy, E_{kink}, is the difference between the energy expectation value of a basis state with a single kink and that of one with no kinks:

$$\begin{aligned} E_{\text{kink}} = &\langle \downarrow(1)\uparrow(2)\uparrow(3)\cdots\uparrow(N-1)\uparrow(N) \\ &\times |\hat{H}| \downarrow(1)\uparrow(2)\uparrow(3)\cdots\uparrow(N-1)\uparrow(N)\rangle \\ &- \langle \uparrow(1)\uparrow(2)\uparrow(3)\cdots\uparrow(N-1)\uparrow(N) \\ &\times |\hat{H}| \uparrow(1)\uparrow(2)\uparrow(3)\cdots\uparrow(N-1)\uparrow(N)\rangle. \end{aligned} \tag{46}$$

The parameter t is the off-diagonal Hamiltonian element connecting a state with no kinks to a state with a single kink

$$\begin{aligned} t = &\langle \downarrow(1)\uparrow(2)\uparrow(3)\ldots\uparrow(N-1)\uparrow(N) \\ &\times |\hat{H}| \uparrow(1)\uparrow(2)\uparrow(3)\ldots\uparrow(N-1)\uparrow(N)\rangle. \end{aligned} \tag{47}$$

[We use the symbol t here because, as we will see in Sec. VII, this number can be viewed as the hopping energy of a kink—it is distinct from the site hopping energy of Eqs. (9) or (14).] The spin-flip operator, $\hat{\sigma}_x(i)$, causes the i^{th} pseudo-spin to flip.

An examination of Eq. (45) will show that this Hamiltonian is isomorphic to that of the Ising model in a transverse magnetic field. it is important to point out that this identification is a result of simply calculating the matrix elements of the microscopic Hamiltonian in the two-state basis; it is not an *a priori* assumption. The parameters which enter the Ising Hamiltonian, E_{kink} (frequently denoted J in the Ising model) and t (which plays the role of the applied transverse magnetic field strength), are calculated directly from the microscopic Hamiltonian for the multicell problem by finding various matrix elements in the two-state basis. Indeed, the importance of this identification for us is simply in reducing the computational task of computing the Hamiltonian matrix elements. Once this identification is made, one need only compute a few elements directly to deduce the value of all other elements in the matrix.

VI. QCA DYNAMICS USING THE TWO-STATE APPROXIMATION

Now that we have calculated the two-state basis vectors and demonstrated the accuracy of the two-state approximation, we can use them to model QCA devices. We consider first the behavior of a wire consisting of eight cells and examine the current densities involved in cell switching. We will then turn our attention to the switching behavior of the most important QCA logic element, the majority logic gate.

A. The eight-cell line

We consider a line of eight ''standard'' cells with a driver on the left end of the line. Figure 9 shows the calculated cell polarizations at various times. Here, the kink reflection, which made it difficult to see the switching behavior in the shorter line of Figs. 4 and 7, occurs at a much latter time. For this reason, it is possible to see cells in the line consecutively switch to match the new direction of the driver cell. For our standard cell, this switching takes approximately 2 ps per cell (this time will decrease for smaller cells). The ballistic nature of kink propagation is clear in the figure. Also, a comparison with Fig. 4 shows that the switching time is nearly 2.5 times as fast as when intercellular

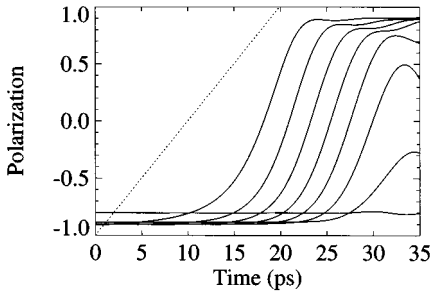

FIG. 9. The dynamic response of a line of eight cells using the two-state approximation. The driver cell changes direction over a period of 20 ps, and the other cells in the line change direction to match it. The polarization kink travels down the wire at a rate of approximately 2 ps per cell.

correlations are neglected. From the relative abruptness of the kink front it is clear that correlations over near neighbors and perhaps next-near neighbors play a role here.

The motion of the kink down the wire raises an interesting question regarding directionality of its motion. Once the kink is several cells away from the driver, how does it ''know'' to continue in the same direction? Using the pseudo-spin language of the last section we can ask the question this way: If at a particular time the line is in state $|\downarrow\downarrow\uparrow\uparrow\uparrow\uparrow\rangle$, is the successor state $|\downarrow\downarrow\downarrow\uparrow\uparrow\uparrow\rangle$ or $|\downarrow\uparrow\uparrow\uparrow\uparrow\uparrow\rangle$?

The answer to this question is that the system is not described by one of these simple states, but is in a linear combination of states. We have seen that kink motion is unidirectional even when we neglect correlations between cells and consider each cell to be described by its own state vector. Thus, for simplicity, consider, within that approximation, the state vector of the cell at the edge of the kink. It is not simply $|\chi'_+\rangle$ or $|\chi'_-\rangle$ (pseudo-spin up or down). It is a linear combination of these: $c_1|\chi'_+\rangle + c_2|\chi'_-\rangle$. The complex ratio of these coefficients determines whether the state is ''up switching to down'' or ''down switching to up.'' This, in turn, determines the direction of kink motion. The ratio of coefficients must be determined by *solving the dynamic problem*; any simple appeal to a static model will prove inadequate.

The nature of this directionality can be illuminated further by considering the particle current density. It is possible to calculate the expectation value of the current density between any two sites within the array. For a given many-cell wave function, this is done by calculating the expectation value of the current density operator

$$\hat{j}(\mathbf{r}) = \frac{1}{2mi}\{\hat{a}^\dagger(\mathbf{r})\nabla\hat{a}(\mathbf{r}) - [\nabla\hat{a}^\dagger(\mathbf{r})]\hat{a}(\mathbf{r})\}. \tag{48}$$

Figure 10 shows a plot of the results of such a current density calculation for the simulation of Fig. 9. The size of the dots at each site represent the expectation value of the charge density on that site, while the length and direction of the arrow between two dots represents the expectation value of the current density between those two dots.

Here, we see that on the right side of the kink (''ahead'' of the kink), the current density is flowing from higher charge densities to lower ones. This acts to depolarize the

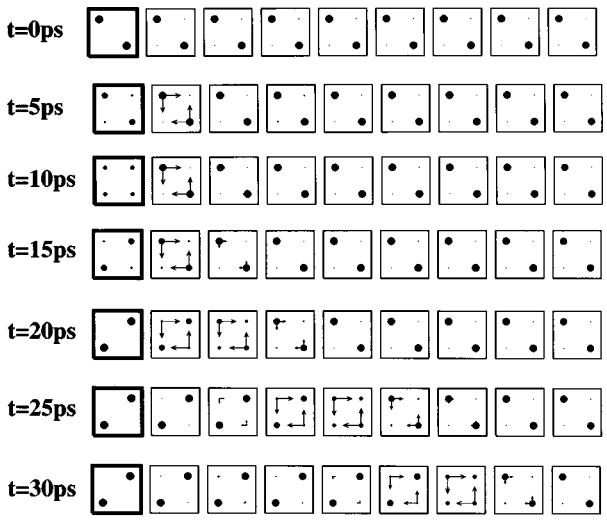

FIG. 10. Calculated particle current. The diameter of each dot is proportional to the charge on the site. Arrows indicate the direction and magnitude of the particle current density. Ahead of the kink (to the right), current density acts to depolarize the cells. Behind the kink (to the left), current density acts to repolarize the cells. This asymmetry in the nature of the current density explains why polarization kinks propagate ballistically down the wire in the desired direction.

cells on the leading edge of the kink. On the left side of the kink (''behind'' the kink), the current density is flowing from lower charge density to higher charge density. This acts to repolarize the cells on the trailing edge of the kink. Thus, the kink has a directionality built into it—a head and a tail. The kink does not get lost. In the absence of dissipation, kink motion proceeds ballistically indefinitely. The presence of dissipation relaxes the kink, and the whole line, to the new ground state.

B. The majority gate

The majority logic gate is the fundamental QCA logic device. Therefore, it is important to verify that a majority logic gate exhibits the correct time-dependent behavior. Figure 11 shows the result of such a time-dependent simulation of a majority logic gate with short wires supplying the inputs and outputs to the device cell. We begin with the system in the ground state. At $t=0$, two of the three inputs to the device (the ones on top and bottom) are in the logical zero state, while the input from the left is in the one state. The device cell and the binary wire connected to the output cell are in the same direction as a majority of the three inputs.

From $t=0$ ps to $t=20$ ps, the direction of the bottom input is continuously switched from $P=-1$ to $P=+1$. This continuous switching occurs between the first two pictures of Fig. 11. The switching of the bottom driver causes the polarization of the binary wire connected to that input to change, just as we saw in the results of Fig. 9. By the time $t=20$ ps, the device cell has begun to switch, indicating that the calculation by the majority logic cell is taking place at that time. By $t=30$ ps, the polarization kink has left the device cell and is traveling down the binary wire connected to the output.

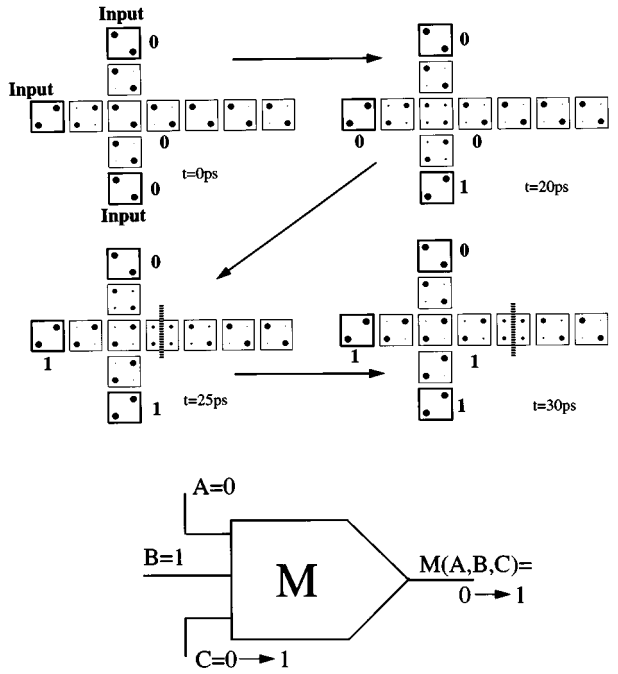

FIG. 11. The switching of a majority gate using the two-state approximation. The bottom input is switched from 0 to 1, and the device cell and output cells change accordingly. The switching occurs without reflection or delay. (b) A schematic diagram of a majority-logic gate showing the change in the input and the corresponding change in the output.

VII. DYNAMICS OF THE SEMI-INFINITE WIRE

Although the two-state approximation dramatically reduces the size of the basis set required to model a QCA device, it is possible to reduce the basis set even further if we exclude those basis vectors with many kinks in the system. For a small but interesting class of problems, like those of kink propagation, we introduce only a single kink into the system by switching the input. It is then unlikely that the system will ever enter the part of the Hilbert space spanned by those basis vectors with many kinks. In addition to reducing the required basis set, this single-kink approximation allows us to introduce a kink-absorbing boundary condition at the end of a wire which can be used both to simulate the behavior of a semi-infinite wire and to crudely introduce energy dissipation into our model. Such a wire will not exhibit any of the kink reflections present in the nondissipative calculations presented above. We will also use this approximation to examine the dynamic response of a binary wire with a spacing error.

A. The single-kink Hamiltonian

The two-state approximation eliminates all of the unnecessary basis states within an individual cell, but there are still many unused basis vectors in the many-cell direct-product space of these two states. Those many-cell basis vectors containing several kinks are unnecessary when modeling a system that contains a single kink, so the next logical reduction of the basis set is to eliminate those direct-product vectors with more than one kink.

If we begin with the pseudo-spin interpretation of the two-state many-cell basis presented in Eq. (43), it is possible to enumerate those basis vectors with no more than one kink. If the driver cell on the left of the wire has a polarization of $+1$, the single basis state with no kinks is:

$$|\Xi_0^+\rangle = |\uparrow(1)\uparrow(2)\uparrow(3)\ldots\uparrow(N-2)\uparrow(N-1)\uparrow(N)\rangle \quad (49)$$

and there are a number of single-kink basis states equal to the number of cells in the line

$$\begin{aligned}
|\Xi_1^+\rangle &= |\downarrow(1)\downarrow(2)\downarrow(3)\cdots\downarrow(N-2)\downarrow(N-1)\downarrow(N)\rangle,\\
|\Xi_2^+\rangle &= |\uparrow(1)\downarrow(2)\downarrow(3)\cdots\downarrow(N-2)\downarrow(N-1)\downarrow(N)\rangle,\\
|\Xi_3^+\rangle &= |\uparrow(1)\uparrow(2)\downarrow(3)\cdots\downarrow(N-2)\downarrow(N-1)\downarrow(N)\rangle,\\
&\vdots\\
|\Xi_{N-1}^+\rangle &= |\uparrow(1)\uparrow(2)\uparrow(3)\cdots\uparrow(N-2)\downarrow(N-1)\downarrow(N)\rangle,\\
|\Xi_N^+\rangle &= |\uparrow(1)\uparrow(2)\uparrow(3)\cdots\uparrow(N-2)\uparrow(N-1)\downarrow(N)\rangle.
\end{aligned} \quad (50)$$

Notice that the i^{th} single-kink basis vector contains a kink to the left of the i^{th} nondriver cell.

If the polarization of the driver cell is -1, the kink-free basis vector is

$$|\Xi_0^-\rangle = |\downarrow(1)\downarrow(2)\downarrow(3)\cdots\downarrow(N-2)\downarrow(N-1)\downarrow(N)\rangle \quad (51)$$

and the single-kink basis vectors are

$$\begin{aligned}
|\Xi_1^-\rangle &= |\uparrow(1)\uparrow(2)\uparrow(3)\cdots\uparrow(N-2)\uparrow(N-1)\uparrow(N)\rangle,\\
|\Xi_2^-\rangle &= |\downarrow(1)\uparrow(2)\uparrow(3)\cdots\uparrow(N-2)\uparrow(N-1)\uparrow(N)\rangle,\\
|\Xi_3^-\rangle &= |\downarrow(1)\downarrow(2)\uparrow(3)\cdots\uparrow(N-2)\uparrow(N-1)\uparrow(N)\rangle,\\
&\vdots\\
|\Xi_{N-1}^-\rangle &= |\downarrow(1)\downarrow(2)\downarrow(3)\cdots\downarrow(N-2)\uparrow(N-1)\uparrow(N)\rangle,\\
|\Xi_N^-\rangle &= |\downarrow(1)\downarrow(2)\downarrow(3)\cdots\downarrow(N-2)\downarrow(N-1)\uparrow(N)\rangle.
\end{aligned} \quad (52)$$

Thus, we can see that the basis set to be used in the single-kink approximation depends on the state of the driver cell associated with the system. There are a total of $2N$ basis vectors associated with both driver polarizations, since the kink-free basis state is also a member of the single-kink basis for the opposite polarization.

Now we will write the Hamiltonian, Eq. (14), in the single-kink basis with a driver of positive polarization, $\{|\Xi_i^+\rangle\}$. In this reduced basis, the Hamiltonian has tridiagonal form and is isomorphic to the Hamiltonian of a particle moving in the tight-binding model. For this reason, it is now helpful to view the polarization kink as a pseudo-particle and to simulate the motion of that pseudo-particle in a way dictated by the tight-binding model and the Hamiltonian elements E_{kink} and t, as defined in Eqs. (46) and (47). The Hamiltonian for a polarization kink as a pseudo-particle in the tight-binding model is

$$\hat{H}_{\text{kink}}=\sum_{i=1}^{N}\hat{n}_{\text{kink}}(i)E_{\text{kink}}+t\sum_{i=1}^{N-1}(\hat{a}^{\dagger}_{\text{kink}}(i)\hat{a}_{\text{kink}}(i+1)+\hat{a}^{\dagger}_{\text{kink}}(i+1)\hat{a}_{\text{kink}}(i)) \tag{53}$$

where $\hat{a}^{\dagger}_{\text{kink}}(k)$ and $\hat{a}_{\text{kink}}(k)$ are the creation and annihilation operators for a kink pseudo-particle to the left of the k^{th} site:

$$\hat{a}^{\dagger}_{\text{kink}}(k)|\uparrow(1)\uparrow(2)\uparrow(3)\cdots\uparrow(k-1)\uparrow(k)\uparrow(k+1)\cdots\uparrow(N-2)\uparrow(N-1)\uparrow(N)\rangle$$
$$=|\uparrow(1)\uparrow(2)\uparrow(3)\cdots\uparrow(k-1)\downarrow(k)\downarrow(k+1)\cdots\downarrow(N-2)\downarrow(N-1)\downarrow(N)\rangle \tag{54}$$

and

$$\hat{a}_{\text{kink}}(k)|\uparrow(1)\uparrow(2)\uparrow(3)\cdots\uparrow(k-1)\downarrow(k)\downarrow(k+1)\cdots\uparrow(N-2)\uparrow(N-1)\uparrow(N)\rangle=|\uparrow(1)\uparrow(2)\uparrow(3)\cdots\uparrow(k-1)\uparrow(k)\uparrow(k+1)\cdots\uparrow(N-2)\uparrow(N-1)\uparrow(N)\rangle. \tag{55}$$

In Eq. (53), $\hat{n}_{\text{kink}}(i)$ is the number operator for a kink on the i^{th} site. When this Hamiltonian is written in the single-kink basis set, the diagonal elements have a value of E_{kink} and the off-diagonal elements connecting neighboring sites have a value of t.

B. Kink absorbing boundary condition: The semi-infinite wire

While the single-kink approximation reduces the required size of the basis set and therefore allows the modeling of larger devices, no additional information would be gained by applying that technique to simply model a longer wire. It is useful, however, in allowing the implementation of method of dissipating energy from the system at the end of the wire. Recent work of Hellums and Frensley, based in part on the quantum transmitting boundary method of Lent and Kirkner, has made it possible to include particle-absorbing boundary conditions at the ends of a wire.[25] We use this boundary condition to absorb the pseudo-particle representing the polarization kink and refer the reader to Ref. 25 for a complete description of the method. Such kink absorption will lower the energy of the system and have the effect of simulating energy dissipation in the calculations.

The particle-absorbing boundary condition is non-Markovian since it includes a convolution integral over the past history of the system. The system of interest is coupled to a semi-infinite kink reservoir, which is capable of absorbing kinks present at the interface between the system and the reservoir. The time-dependent Schrödinger equation for the combination of these two systems is

$$i\hbar\frac{\partial}{\partial t}\begin{bmatrix}\psi_S\\ \psi_R\end{bmatrix}=\begin{bmatrix}H_s & H_{iR}^{\dagger}\\ H_{iR} & H_{rR}\end{bmatrix}\begin{bmatrix}\psi_S\\ \psi_R\end{bmatrix}. \tag{56}$$

Here, Ψ_s is the state of the modeled system, Ψ_r is the state of the kink reservoir, H_s is the Hamiltonian of the system, H_{rR} is the Hamiltonian of the reservoir, and H_{iR} is the interaction Hamiltonian coupling the two systems. After using Laplace transforms to eliminate Ψ_{rR}, the time-dependent Schrödinger equation becomes

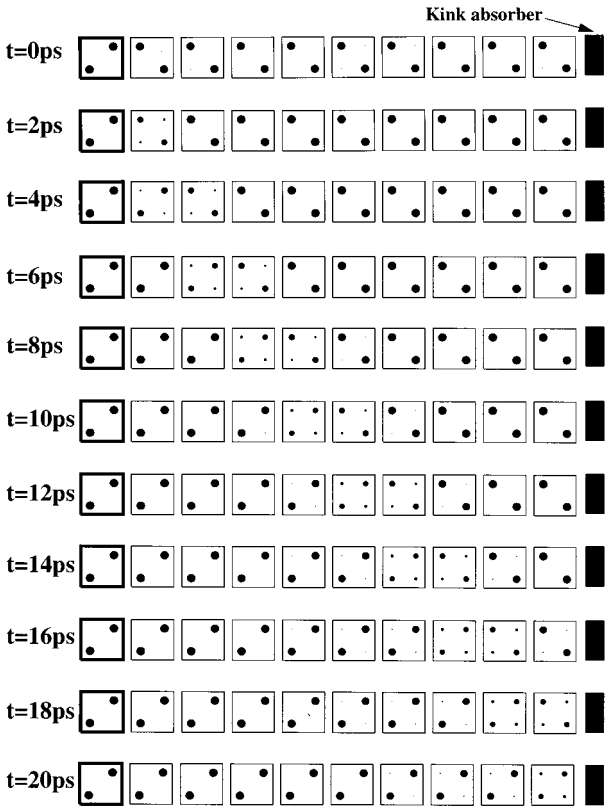

FIG. 12. Dynamic response of a single-kink wire with a kink absorber at the end. The kink propagates at a rate of 2 ps per cell and has completely left the system by $t=20$ ps.

$$i\hbar\frac{\partial\psi_s}{\partial t}=H_s\psi_s(t)+H_{iR}^{\dagger}\left[\int_0^t G_R(t-\tau)H_{iR}\psi_s(\tau)d\tau+i\hbar G_R(t)\psi_{rR}(0)\right], \tag{57}$$

where $G_R(t)$ is the propagator for the reservoir, which is a function of the coupling between cells in the reservoir.

We solve Eq. (57) using the values for H_s from the tight-binding model for polarization kinks. When this method is used to model a line of QCA cells, the results are those shown in Fig. 12. The driver cell is changed from a polarization of -1 to a polarization of $+1$, and all of the other cells in the line react to this change. The kink propagates down the wire at a rate of approximately 2 ps per cell, and no reflection occurs at the end of the wire. The kink has essentially left the wire by $t=20$ ps, allowing it to dissipate energy and settle into the new switched ground state.

C. Spacing error

Landauer has objected that an error in the intercellular spacing within a QCA wire would result in wire failure.[18] His argument is that if a larger-than-standard gap were to occur between cells $k-l$ and k, the effect of cell $k+l$ on cell k would be greater than that of cell $k-l$. The result, he suggests, is that the line could not be switched to a new state because the old state, represented by cell $k+l$, would keep cell k in from switching.

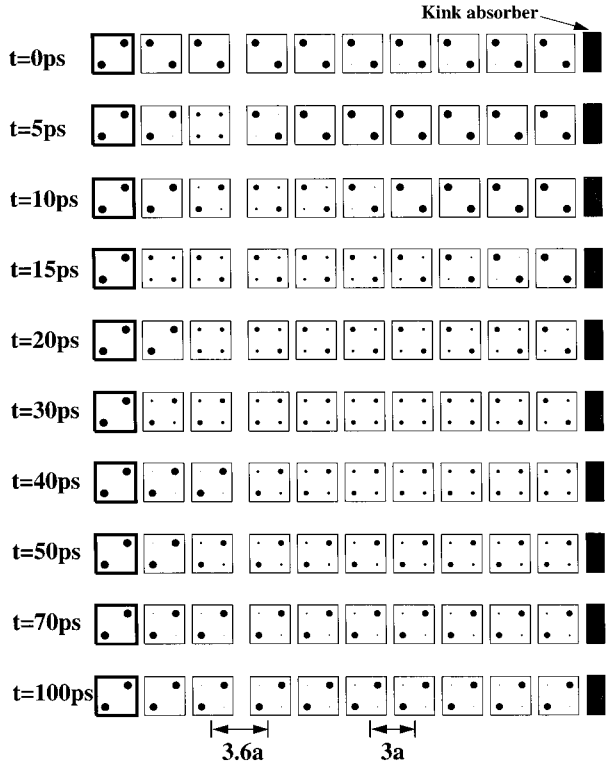

FIG. 13. Dynamic response of a single-kink wire with a spacing error and a kink absorber at the end. The spacing error causes a delay, but the wire still operates correctly.

We have performed a time-dependent solution of such a system using the single-kink approximation and found that the line indeed switches. The result of this calculation is shown in Fig. 13, in which a wire with a 20% spacing error (a rather larger error than one would likely expect) between two of the cells near the middle of the wire is being studied. According to the objection the polarization, kink should stop when it reaches the gap, since the cell on the other side of the gap is more strongly influenced by its nonswitched neighbor. While the spacing error causes some partial reflections of the kink, with a resulting delay in the time it takes to switch the entire wire, the wire does switch to match the driver cell. A spacing error acts as a small barrier for kink propagation. What the calculation illustrates is that even a very large spacing error acts as a relatively small barrier which does not keep the system from switching.

The spacing error problem is a specific case of Landauer's more general objection that QCA systems suffer from a lack of unidirectionality because inside the array cells with ''old'' information have as much weight as cells with ''new'' information. The calculations shown here illustrate that the ballistic nature of kink motion, even in the absence of dissipation, are sufficient in many systems to provide the unidirectionality desired. More fundamentally we believe this argument is invalid because the new information presented at the inputs causes the ground state of the system to change. It is this effect, rather than the details of the temporal evolution, that are the heart of the matter. Unidirectionality is effected because of the breaking of the symmetry between input and output—inputs are held fixed and outputs are not.

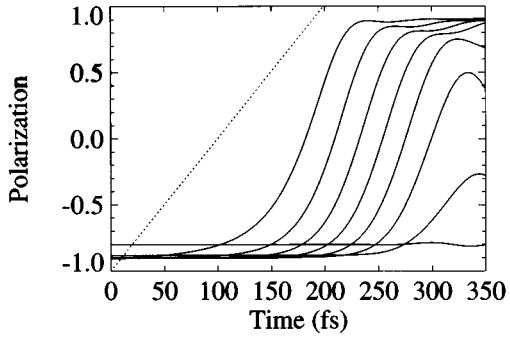

FIG. 14. Dynamic response of an eight-cell macromolecular wire using the two-state approximation. Kink propagation requires 20 fs, which is an improvement by a factor of 100 over the semiconductor cells.

The only relevant issue beyond that is the issue of metastability—will the system succeed in reaching the ground state in a reasonable time? The spacing error problem is important not from the point of view of unidirectionality, but from the point of view of metastability. Landauer is correct in that a spacing error could, in principle, be a source of a metastable hangup. The question becomes a quantitative one—is the kinetic barrier between the state just after the input is switched and the desired ground state *large enough* to keep the system from reaching its ground state, leaving it stuck in a metastable excited state? Such a quantitative question can only be answered by a quantitative calculation such as this one. In this case the answer is that even a fairly large spacing error does not cause a problem (of course, a bizarrely large spacing error would). There are certain instances, such as fanout, to which Landauer also correctly points, for which metastability could be a much more serious problem. We address that issue elsewhere in the context of gradual adiabatic switching.[26]

VIII. MACROMOLECULAR CELLS

As stated above, the speed of QCA devices improves as the size decreases. At the present time, the long-term goal of such shrinking is a macromolecular implementation, in which the QCA cells are formed by self-assembling molecules.[27] It is expected that such cells will be at least ten times smaller than the ''standard'' semiconductor cells, will have a dielectric constant of 1, and electrons in those cells will have the effective mass of free electrons. We investigate the dynamic behavior of these cells to estimate the amount of improvement that can be expected by their use.

The two-state calculations of Fig. 9 were repeated using the parameters described above for macromolecular cells. The results of this calculation are shown in Fig. 14, and demonstrate that the use of macromolecular cells improves the switching speed of a cell by a factor of 100 over that of the ''standard'' cell. Instead of 2 ps per cell, these devices now switch at 20 fs per cell.

Repeating the single-kink calculations of Fig. 12 for macromolecular cells yields the result shown in Fig. 15. This calculation also results in an improvement of the switching speed by a factor of 100 over that of a ''standard'' cell.

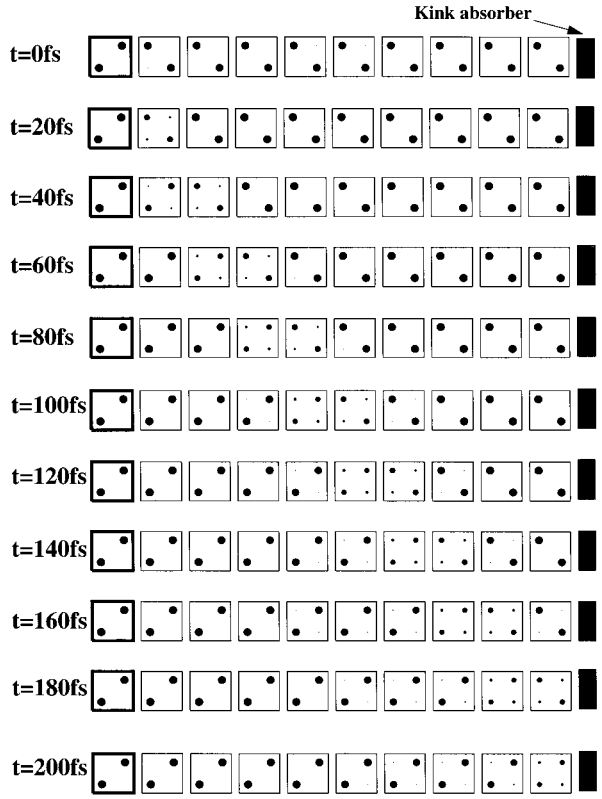

FIG. 15. Kink propagation in a macromolecular wire using the single-kink approximation and a kink absorber at the end of the wire. The polarization kink propagates across one cell in approximately 20 fs and leaves the system by $t=200$ fs.

In addition to these improvements in speed, corresponding improvements in the possible operating temperature are observed. While standard cells are calculated to operate satisfactorily at temperatures up to 5 K, the larger Coulombic energies present in macromolecular cells make it possible for them to operate at or above room temperature. This combination of an improvement in speed and in operating temperature makes implementation of macromolecular cells a very attractive goal.

IX. CONCLUSIONS

We examined the dynamics of isolated QCA arrays with a particular focus on assessing the intrinsic switching behavior. Dissipative coupling to thermal reservoirs will likely be important in real arrays. This coupling could result in useful switching times for real devices that are faster (for strong dissipative coupling) or slower (for very weak dissipative coupling) than the intrinsic limits we have examined. We have also studied methods to reduce the size of the basis set required to accurately model large QCA devices.

Clearly, fabrication of these devices remains the largest challenge to the realization of QCA arrays, but current techniques in nanofabrication make this realization quite possible.[28] Other challenges, such as detecting the presence or absence of a single electron at the output,[20,29] and maintaining a uniform cell occupancy throughout the array,[30,31] have already been addressed.

While this paper has concentrated on switching the devices only by varying the polarization of the driver cell, it is also possible to lower and raise the barriers within each cell so as to facilitate correct switching. If the barriers are lowered, the confinement of the electrons on each site will be relaxed, and the polarization of the cells will decrease. The driver cell can then be switched, and the barriers raised again. The array will then ''recrystallize'' in its new ground state without any excess ''kink energy'' ever being introduced to the system. If the switching is done slowly enough, the adiabatic theorem guarantees that the system can be maintained at all times in its instantaneous ground state, eliminating any metastability problems. Such adiabatic switching will be discussed more thoroughly elsewhere.[26]

ACKNOWLEDGMENTS

We gratefully acknowledge stimulating conversations with members of the Notre Dame Nanoelectronic Group, especially Wolfgang Porod. We also thank Professor Thomas Kaplan of Michigan State University for his help in identifying the connection to the Ising model in a transverse field. This work was supported in part by the Advanced Research Projects Agency and the Office of Naval Research. This material is based in part upon work supported under a Center for Applied Mathematics Graduate Fellowship.

[1] For a recent overview see, *Nanostructures and Mesoscopic Systems*, edited by W. P. Kirk and M. A. Reed (Academic, Boston, 1992).
[2] R. Landauer, Phys. Today **42**, 119 (1989).
[3] D. C. Miller, R. K. Lake, and S. Datta, in *Nanostructure Physics and Fabrication*, edited by M. A. Reed and W. P. Kirk (Academic, Boston, 1989).
[4] C. S. Lent, P. Douglas Tougaw, and Wolfgang Porod, Appl. Phys. Lett. **62**, 714 (1993).
[5] C. S. Lent, P. Douglas Tougaw, Wolfgang Porod, and Gary H. Bernstein, Nanotechnology **4**, 49 (1993).
[6] P. Douglas Tougaw, C. S. Lent, and Wolfgang Porod, J. Appl. Phys. **74**, 3558 (1993).
[7] C. S. Lent and P. Douglas Tougaw, J. Appl. Phys. **74**, 6227 (1993).
[8] P. Douglas Tougaw and C. S. Lent, J. Appl. Phys. **75**, 1818 (1994).
[9] C. S. Lent and P. Douglas Tougaw, J. Appl. Phys. **75**, 4077 (1994).
[10] T. Toffoli and N. Margolus, *Cellular Automata Machines: A New Environment for Modeling* (MIT, Cambridge, MA, 1987).
[11] L. D. Chua and L. Yang, IEEE Trans. Circuits Syst. **35**, 1257 (1988); *ibid.* **35**, 1273 (1988).
[12] R. T. Bate, Bull. Am. Phys. Soc. **22**, 407 (1977).
[13] J. N. Randall, M. A. Reed, and G. A. Frazier, J. Vac. Sci. Technol. B **7**, 1398 (1989).
[14] D. K. Ferry, L. A. Akers, and E. W. Greeneich, *Ultra Large Scale Interconnected Microelectronics* (Prentice Hall, Englewood Cliffs, NJ, 1988).
[15] J. N. Randall, A. C. Seabaugh, Y.-C. Kao, J. H. Luscombe, and B. L. Newell, J. Vac. Sci. Technol. B **9**, 2893 (1991).
[16] *Granular Nanoelectronics*, edited by D. K. Ferry, J. R. Barker, and C. Jacoboni (Plenum, New York, 1991).
[17] D. Biafore, Physical D **70**, 415 (1994).
[18] R. Landauer, *Ultimate Limits of Fabrication and Measurement*, edited by M. E. Welland (Kluwer, Dordrecht, 1994).
[19] T. Tanamoto, R. Katoh, and Y. Naruse, Jpn. J. Appl. Phys. **33**, 1502 (1994).
[20] Noninvasive probing of single-electron charging in a semiconductor quantum dot has recently been reported by M. Field, C. G. Smith, M. Pepper,

J. E. F. Frost, G. A. C. Jones, and D. G. Hasko, Phys. Rev. Lett. **70**, 1311 (1993).
[21] We take E_Q to be the Coulomb energy of two electrons separated by one-third the dot diameter D, a physically reasonable first approximation.
[22] Craig S. Lent, in *Nanostructures and Mesoscopic Systems*, edited by W. P. Kirk and M. A. Reed (Academic, Boston, 1992), p. 183.
[23] We have explored the phase space of Hamiltonian parameters in Ref. 7 and conclude that cell polarization does not rely on a critical balancing of these parameters, but is a general characteristic of the cell design.
[24] Hereinafter we will refer to the kink in polarization without the qualifying quotation marks.
[25] J. R. Hellums and W. R. Frensley, Phys. Rev. B **49**, 2904 (1994).
[26] C. S. Lent and P. D. Tougaw (unpublished).
[27] For a review of the current state, see *Molecular Electronics*, edited by Geoffrey J. Ashwell (Wiley, New York, 1992).
[28] For a recent collection of quantum dot papers, see a special issue of Physica B on ''The Physics of Few-Electron Nanostructures,'' edited by L. J. Geerligs, C. J. P. M. Harmans, and L. P. Kouwenhoven, Physica B **189** (1993).
[29] M. Kemerink and L. W. Molenkamp, Appl. Phys. Lett. **65**, 1012 (1994).
[30] R. C. Ashoori, H. L. Stormer, and J. S. Weiner, Physica B **184**, 378 (1993); R. C. Ashoori, H. L. Stormer, J. S. Weiner, L. N. Pfeiffer, K. W. Baldwin, and K. W. West, Physica B **71**, 613 (1993).
[31] The ability to control quantum dot occupancies over as many as 10^8 dots using a back-gating technique has recently been reported by B. Meurer, D. Heitmann, and K. Ploog, Phys. Rev. Lett. **68**, 1371 (1992).